ArXiv:Astro-ph, Oct 26-30, 2015

Обзор от Сильченко О.К.

Astro-ph: 1510.07657

Astronomy & Astrophysics manuscript no. pcigale˙def
October 28, 2015

The imprint of rapid star formation quenching on the spectral energy distributions of galaxies.

L. Ciesla[1,2,3], A. Boselli[4], D. Elbaz[3], S. Boissier[4], V. Buat[4], V. Charmandaris[2,1], C. Schreiber[3], M. Béthermin[5], M. Baes[6], M. Boquien[7], I. De Looze[8,7,6], J.A. Fernández-Ontiveros[9], C. Pappalardo[10], L. Spinoglio[9], S. Viaene[6].

Всеволновая SED, SFH с обрывом

Table 1: Broad-band filter-set used in this paper.

Telescope/Camera	Filter Name	λ_{mean} (μm)	Ref.
GALEX	FUV	0.153	a
	NUV	0.231	a
	U	0.365	b
	B	0.44	b
SDSS	g	0.475	a
	V	0.55	b
SDSS	r	0.622	a
SDSS	i	0.763	a
2MASS	J	1.25	b
	H	1.65	b
	Ks	2.1	b
Spitzer	IRAC1	3.6	c
	IRAC2	4.5	c
	IRAC4	8	d
WISE	3	12	d
	4	22	d
	MIPS1	24	e
	MIPS2	70	e
Herschel	PACS green	100	f
	PACS red	160	f
	PSW	250	g
	PMW	350	g
	PLW	500	g

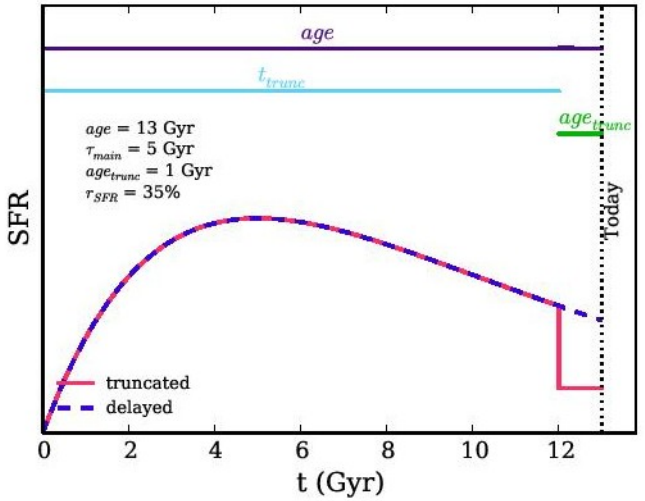

Fig. 1: Illustration of the truncated delayed SFH implemented in CIGALE. The purple dashed line represents a normal delayed SFH with τ_{main}=5 Gyr, without truncation. The red solid line is the truncated delayed SFH.

Варьировались, в частности, давность и амплитуда обрыва SFH

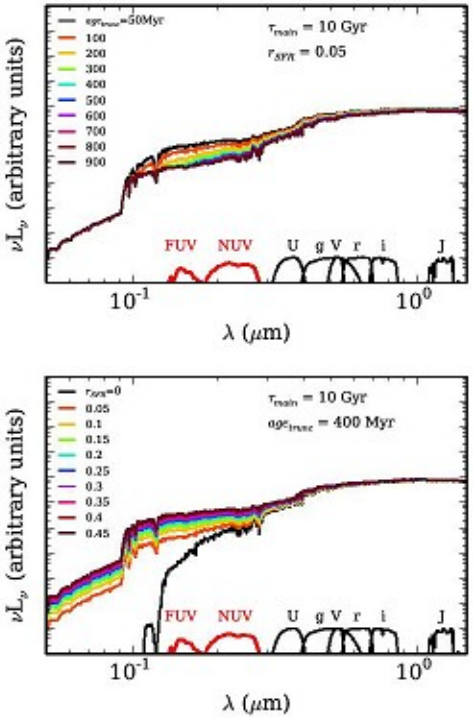

Fig. 3: Impact of the two parameters, age_{trunc} (upper panel) and r_{SFR} (lower panel), on the SED considering a τ_{main} of 10 Gyr. SEDs are color coded according to the value of the free parameter. For clarity, we only show in this plots models with r_{SFR} lower than 0.45. At the bottom of each panel, we show the filters of GALEX (red), SDSS, and 2MASS.

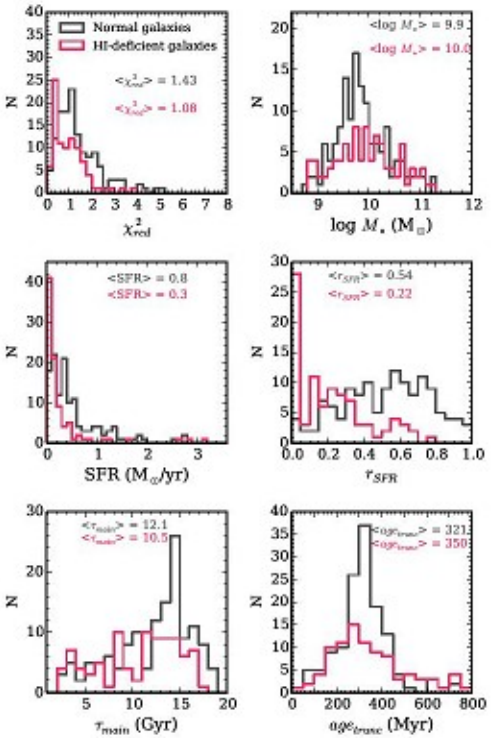

Fig. A.1: Distribution of the output parameters obtained from the SED fitting procedure with CIGALE. The results for the normal galaxy sample are shown in grey while the results for the HI-deficient sample are shown in red.

Конкретно ультрафиолет требует обрыва SFH для галактик с дефицитом газа

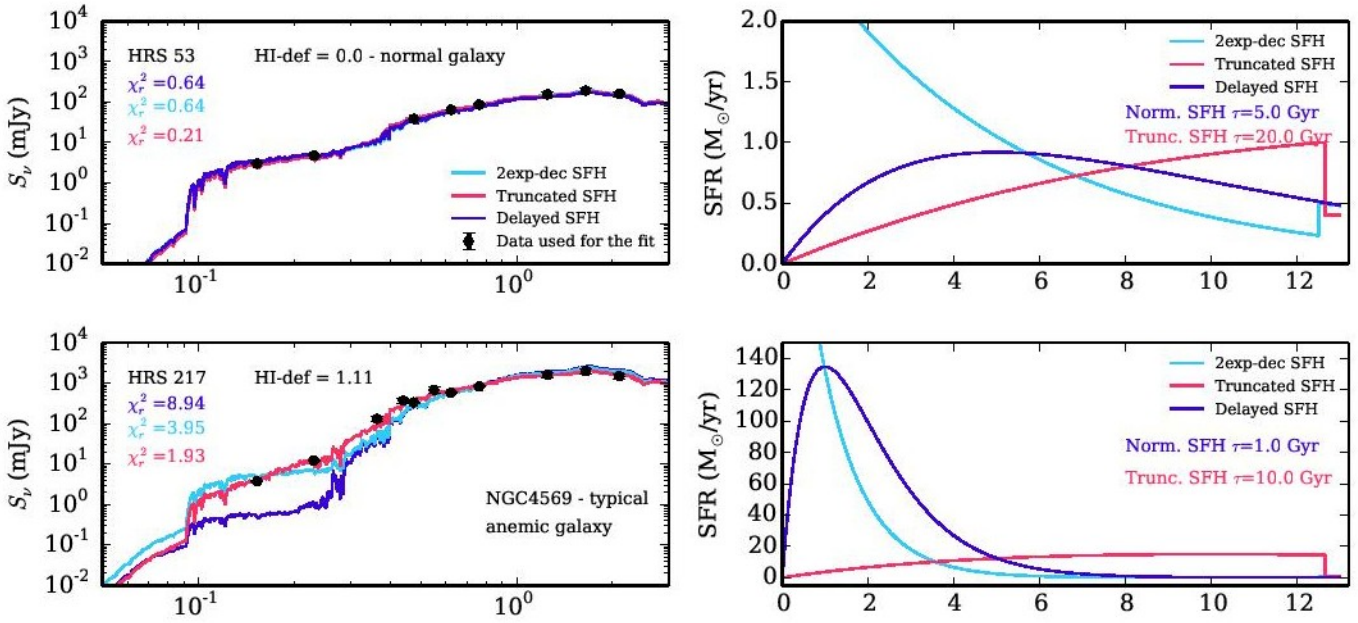

Astro-ph: 1510.08060

Draft version October 29, 2015
Preprint typeset using LaTeX style emulateapj v. 05/12/14

ON THE PERSISTENCE OF TWO SMALL-SCALE PROBLEMS IN ΛCDM

Marcel S. Pawlowski[1], Benoit Famaey[2], David Merritt[3], and Pavel Kroupa[4]
[1]Department of Astronomy, Case Western Reserve University,
10900 Euclid Avenue, Cleveland, OH, 44106, USA
[2]Observatoire astronomique de Strasbourg, Université de Strasbourg,
CNRS, UMR 7550, 11 rue de l'Université, F-67000 Strasbourg, France
[3]School of Physics and Astronomy and Center for Computational Relativity and Gravitation,
Rochester Institute of Technology, 84 Lomb Memorial Drive, Rochester, NY 14623, USA
[4]Helmholtz-Institut für Strahlen- und Kernphysik, Rheinische Friedrich-Wilhelms-Universität Bonn,
Nussallee 14-16, D-53115 Bonn, Germany
Draft version October 29, 2015

ABSTRACT

We investigate the degree to which the inclusion of baryonic physics can overcome two long-standing problems of the standard cosmological model on galaxy scales: (i) the problem of satellite planes around Local Group galaxies, and (ii) the "too big to fail" problem. By comparing dissipational and dissipationless simulations, we find no indication that the addition of baryonic physics results in more flattened satellite distributions around Milky-Way-like systems. Recent claims to the contrary are shown to derive in part from a non-standard metric for the degree of flattening, which ignores the

Проблема спутников в LCDM!

2. SATELLITE PLANE PROBLEM

The satellite plane problem for the eleven classical MW satellite galaxies[1] can be summarized as follows: The (three-dimensional) positions of the MW satellite galaxies are distributed such that they all lie close to one common plane which has a root-mean-square (rms) height of 19.6 kpc and a rms minor-to-major axis ratio of $c/a = 0.182$. Most of these satellites have orbital planes which are closely aligned with the plane defined by their position and they also share the same orbital direction (they co-orbit). This is indicated by the close clustering of 8 out of 11 orbital poles (directions of angular momentum) close to one normal vector describing the orientation of the best-fitting plane. In addition, one of the remaining three of the 11 orbital poles is directed along the opposite pole (i.e. retrograde relative to the 8 others).

Therefore, the defining characteristics of the satellite plane problem are that:

- the satellites are distributed in a highly flattened, *planar* structure in three-dimensional space,
- the *majority* of the satellites *co-orbit* in the same sense,
- and these satellites orbit *within* the plane, indicating that the plane is not just a transient alignment.

Плоскость спутников с ребра

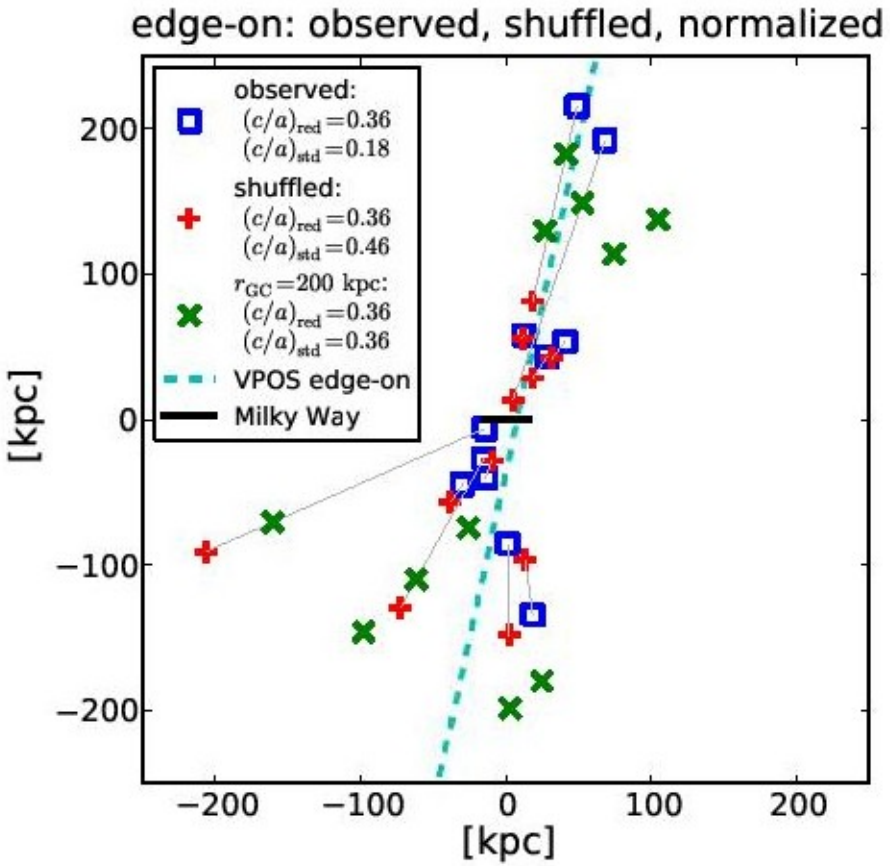

Концентрация полюсов орбит спутников и много чего еще

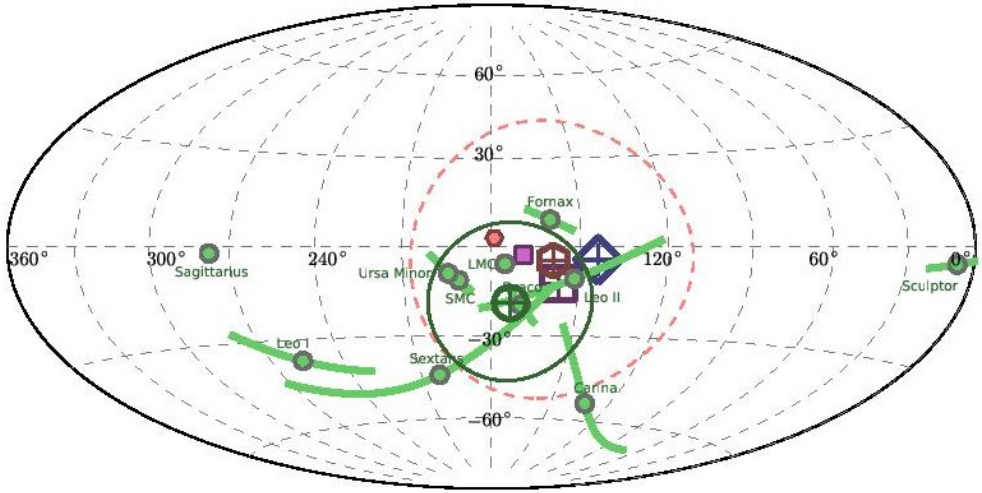

Figure 2. *Upper panel*: The orbital poles of the 11 brightest ('classical') MW satellites for which PMs are measured (green dots with green great-circle segments indicating the 1σ-uncertainties) are plotted in Galactic coordinates. Also shown are the normal to the best-fitting plane of the 11 classical MW satellites (light magenta square), the VPOS normal (dark magenta open square with plus sign), the normal to the plane fitted to the MW globular clusters classified as young halo objects (blue open diamond with plus sign), the average orbital pole direction (dark green open circle with plus sign, using the most-recent determination from an updated list of streams in Pawlowski & Kroupa 2014), the average direction of all MW stream normals (dark red hexagon with plus sign, from Pawlowski & Kroupa 2014), and the stream normal of the Magellanic Stream (small light-red hexagon). *Lower panel*: The same orbital poles are plotted in a

Сравнение с LCDM-моделями

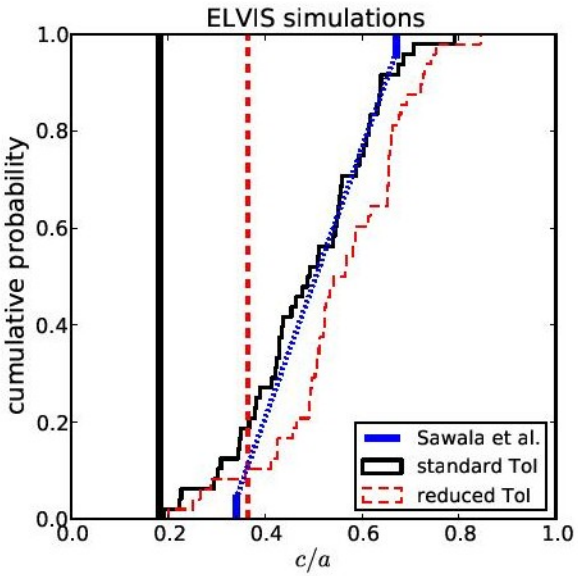

Figure 4. Cumulative distribution of $(c/a)_{\rm red}$ and $(c/a)_{\rm std}$ axis ratios as in Fig. 1, but for satellites in the ELVIS suite of dark-matter-only simulations of Local Group analogs (Garrison-Kimmel et al. 2014). The blue lines indicate the range of $(c/a)_{\rm red} = 0.34$ to 0.67 reported by S14 for the hydrodynamical simulations including baryonic physics, determined using the reduced TOI. We do not know the shape of the cumulative distribution between these points.

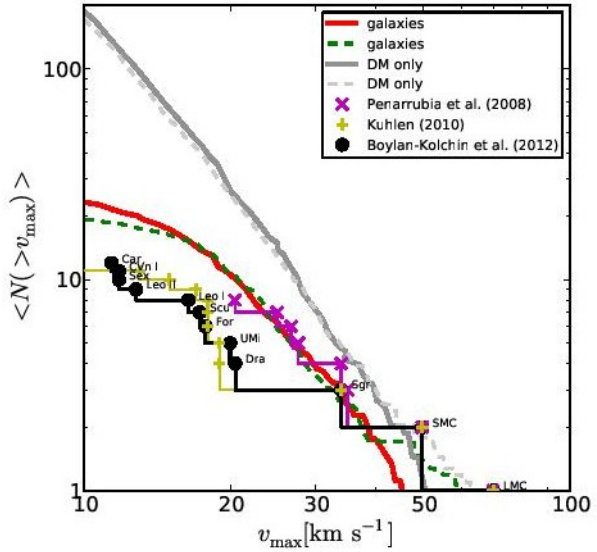

Figure 5. Cumulative number of satellites (sub-halos or galaxies) as a function of their maximum circular velocity $v_{\rm max}$. The data for the EAGLE simulations as presented in S14 were extracted from their figure 3. These are averages of the 12 simulations of Local Group equivalents analyzed by S14. The two upper (grey) lines show the cumulative sub-halo number for their dark-matter-only simulations, the two lower (red and green) lines the cumulative number of luminous satellite galaxies for the MW and M31 equivalents. The magenta crosses are the old $v_{\rm max}$ estimates for

Astro-ph: 1510.08147

CHRONOGRAPHY OF THE MILKY WAY'S HALO SYSTEM WITH FIELD BLUE HORIZONTAL-BRANCH STARS

Rafael M. Santucci
Departamento de Astronomia - Instituto de Astronomia, Geofísica e Ciências Atmosféricas, Universidade de São Paulo, São Paulo, SP 05508-900, Brazil

Timothy C. Beers, Vinicius M. Placco, Daniela Carollo
Department of Physics and JINA Center for the Evolution of the Elements, University of Notre Dame, 225 Nieuwland Science Hall, Notre Dame, IN 46556, USA

Silvia Rossi
Departamento de Astronomia - Instituto de Astronomia, Geofísica e Ciências Atmosféricas, Universidade de São Paulo, São Paulo, SP 05508-900, Brazil

Young Sun Lee
Department of Astronomy and Space Science, Chungnam National University, Daejeon 34134, Republic of Korea

Pavel Denissenkov
Department of Physics & Astronomy, University of Victoria, Victoria, BC, V8W3P6, Canada

Jason Tumlinson
Space Telescope Science Institute, Baltimore, MD 21218, USA

Patricia B. Tissera
Departamento de Ciencias Fisicas and Millennium Institute of Astrophysics, Universidad Andres Bello, Av. Republica 220, Santiago, Chile

Наблюдения и модели: 4700 BHB

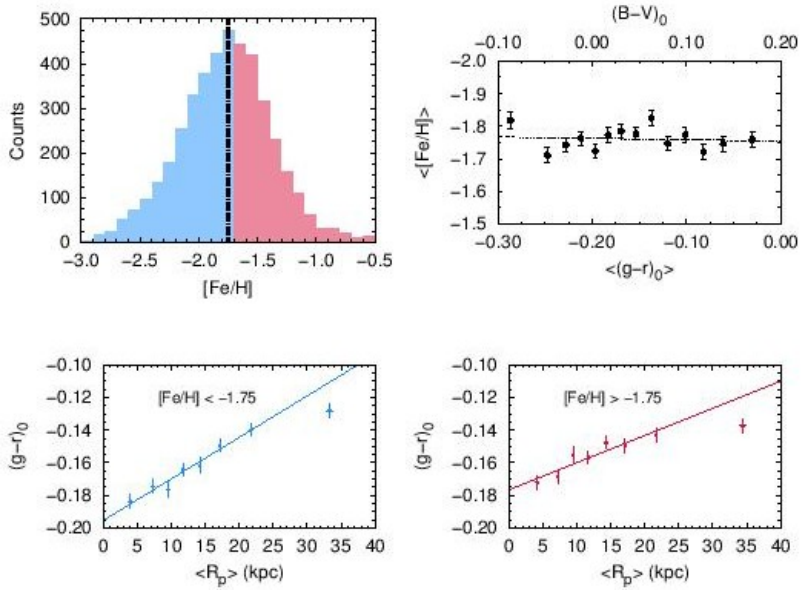

FIG. 2.— *Top-left panel*: Distribution of metallicity, [Fe/H], for the BHB sample. The distribution is divided into two equal parts (at [Fe/H]= −1.75), color-coded according to [Fe/H]. *Top-right panel*: The mean [Fe/H]as a function of mean $(g-r)_0$ color over the full extent of our selected color window, $-0.30 < (g-r)_0 < 0.00$. There is no variation of $\langle$[Fe/H]$\rangle$ with $\langle\ (g-r)_0\ \rangle$. *Lower panels*: Robust fits to $(g-r)_0$ vs. R_p for both metallicity intervals, color-coded according to the distribution shown in the top-left panel. Note that the color shift with distance is similar for both metallicity intervals, but the higher interval exhibits a slightly shallower slope. The points in these panels represent an average of 300 BHBs in each bin; error bars are the standard errors in the mean. The outer-most point in both panels is located at distances where the contribution from resolved substructures becomes substantial, giving rise to the

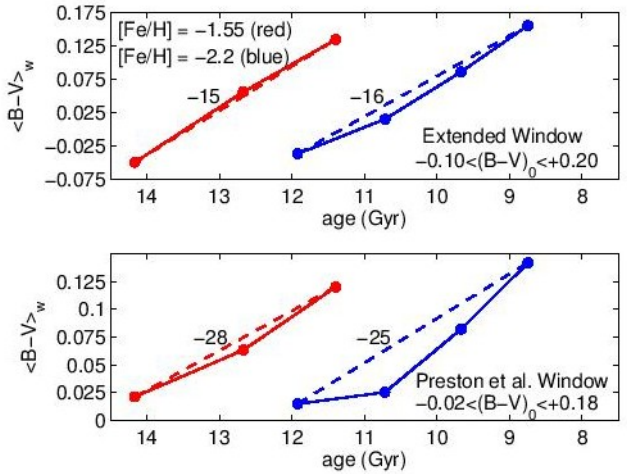

FIG. 4.— The dependencies of $\langle B-V\rangle_w$ on the HB age for two metallicities (indicated in the upper panel) estimated from our HB population-synthesis simulations (filled circles connected by solid lines). Dashed lines and the numbers next to them give the mean slopes $(\Delta t_9/\Delta\langle B-V\rangle_w)$ of the dependencies. The results are shown for the extended window (upper panel) and the original Preston et al. window (lower panel).

Карта возрастов звезд BHB поля

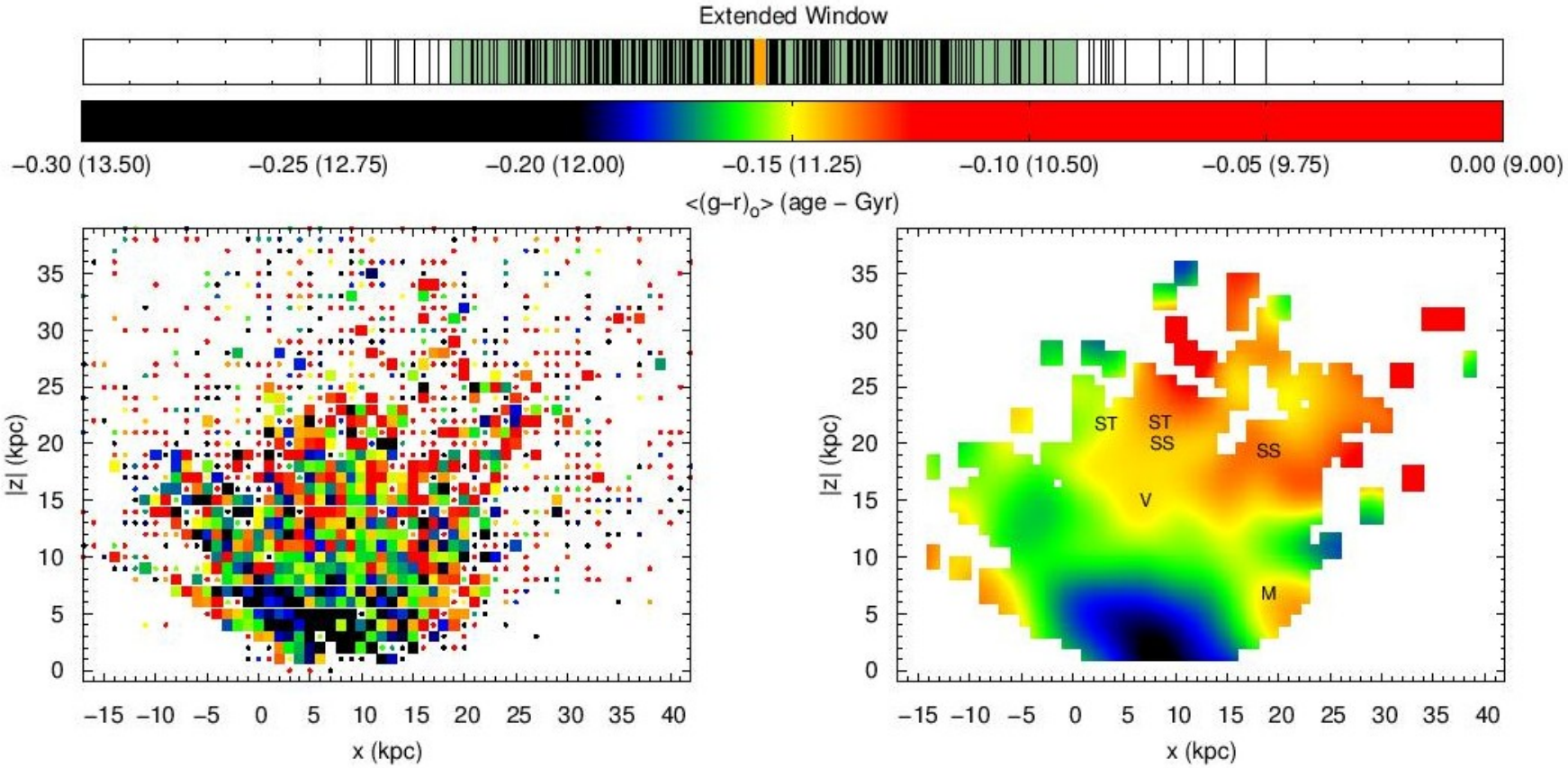

Оригинальная по-звездная

Сглаженная